

PACS numbers: 81.05.Je; 72.10.Fk; 63.20.kp
DOI: 10.1070/QE2013v043n03ABEH015136

Structure of crystalline oxide ceramics studied by phonon spectroscopy

A.A. Kaminskii, A.V. Taranov, E.N. Khazanov

Abstract. **This paper describes a method for gaining detailed insight into the structure and phonon spectrum of polycrystalline oxide ceramics. We examine how the diffusion coefficient of subterahertz phonons is related to the properties of a system of grain boundaries and to the grain size and structure and demonstrate that the temperature dependence of the phonon diffusion coefficient at liquid-helium temperatures is determined by the spectral properties of the intergranular layer, which allows one to estimate the volume-averaged intergranular layer thickness and acoustic impedance. We also analyse the effect of plastic deformation via twinning on the formation of the structure of grains and intergranular layers, which determine the thermophysical, acoustic and optical properties of ceramic materials.**

Keywords: *oxide ceramics, phonons, grain boundary, twinning.*

1. Introduction

Interest in the detailed structure of ceramics stems, on the one hand, from their new functional properties related to their micro- and nanostructure. On the other hand, ceramic fabrication processes are highly dependent on the ability to control the phase composition of the material, the grain size and orientation and the grain boundary structure, which determine the physical properties of the ceramic [1, 2].

Structural studies of advanced crystalline ceramics by transmission electron microscopy demonstrate the presence of continuous intergranular layers a few nanometres in thickness [3]. However, electron and atomic force microscopies probe a limited volume of material, insufficient for assessing average characteristics of intergranular layers and their influence on the physical properties of the material [4]. At the same time, detailed information about the structure of ceramic materials can be obtained by analysing phonon transport characteristics when the phonon wavelength ($\lambda_{ph} \approx 10-50$ nm) is comparable to the dimensions of microstructural components of the ceramic (grain boundaries, pores and second-phase nanoinclusions).

A.A. Kaminskii A.V. Shubnikov Institute of Crystallography, Russian Academy of Sciences, Leninsky prosp. 59, 119333 Moscow, Russia; e-mail: Kaminalex@mail.ru;
A.V. Taranov, E.N. Khazanov V.A. Kotel'nikov Institute of Radio Engineering and Electronics, Russian Academy of Sciences, Mokhovaya ul. 11/7, 125009 Moscow, Russia; e-mail: taranov@cplire.ru

Received 24 December 2012; revision received 6 February 2013
Kvantovaya Elektronika **43** (3) 282–287 (2013)
Translated by O.M. Tsarev

At low phonon temperatures (energies), where there are conditions for competition between the elastic and inelastic phonon scattering times (τ_0 and τ^*, respectively), phonon transport in materials containing structural defects can be described by a wide variety of regimes [5]. The most informative regime for analysing the influence of structural defects on the key features of phonon transport is classic diffusion, where weakly nonequilibrium phonons propagating through a material are elastically scattered by structural defects and there are no inelastic phonon–phonon interaction processes. If the observation time meets the inequality $t < \tau^*$, such a regime develops when the condition $\tau_0 \ll \tau_b \ll \tau^*$ is satisfied (where τ_b is the ballistic propagation time of phonons in the material). These conditions are as a rule met at liquid-helium temperatures (2–4 K) for almost all dense dielectric oxide materials containing defects. Such materials include, in addition to ceramics, substitutional solid solutions and any materials containing structural defects (extended or one-dimensional) or excitations comparable in energy to phonons [6–8].

The objective of this work was to investigate the specific features of the transport characteristics of subterahertz phonons and examine how these characteristics are related to the structure of grains and grain boundaries and the fabrication conditions of polycrystalline ceramic materials with the aim of optimising the thermophysical, acoustic and optical properties of such ceramics.

2. Experimental technique

The technique used for structural characterisation of ceramics was worked out at the V.A. Kotel'nikov Institute of Radio Engineering and Electronics, Russian Academy of Sciences, and is a development of the heat pulse method [9]. It builds on measurements of temperature-dependent transport characteristics of weakly nonequilibrium thermal phonons in a diffusion regime at liquid-helium temperatures. Heating a metallic (Au) film of a phonon injector to a temperature T_h such that $\Delta T = T_h - T_0 \ll T_0$ does not require T_h measurement (which is a rather challenging problem) and allows one to study temperature-dependent scattering characteristics by varying the thermostat temperature T_0. Under such conditions, inelastic phonon–phonon processes can be neglected, and scattering efficiency is only determined by the structure of the material. Nonequilibrium-phonon pulses that are detected by a superconducting bolometer (Sn, In) on the side opposite to the injector are well described by a solution to the diffusion equation

$$\frac{\partial^2 T}{\partial x^2} = \frac{1}{D}\frac{\partial T}{\partial t}, \qquad (1)$$

where $D = K/c_V$ is the diffusion coefficient; K is the thermal conductivity of the material; and c_V is its heat capacity. The measurable parameter is the time it takes for the diffusion signal to reach a maximum: $t_m = L^2[2D(T)]^{-1}$ (planar diffusion source), where $D(T) = lv/3$; L is the size of the specimen; l is the mean free path of nonequilibrium phonons; and v is the polarisation-averaged sound velocity. The feasibility of the diffusion regime in ceramic materials at liquid-helium temperatures was substantiated and demonstrated by Ivanov et al. [10]. The technique is sensitive to even slight changes in the structure of ceramics and allows one to estimate the volume-averaged acoustic impedance and intergranular layer thickness [11].

As shown in model experiments aimed at assessing phonon–impurity interaction [6], the frequencies of the phonons responsible for the maximum in the diffusion signal measured by the bolometer correspond to $\hbar\omega \approx (3–4)k_BT$ (where k_B is the Boltzmann constant), which allows phonon transport to be analysed within a one-particle model.

Figure 1 presents scanning electron microscopy images of fracture surfaces of different ceramics. The samples are seen to have a dense polycrystalline structure. At liquid-helium temperatures, the mean free path of thermal phonons in dielectric single crystals is usually a fraction of a centimetre. Therefore, when the condition $l/R \gg 1$ is met (where R is the average grain size of the ceramic), the phonon transport mechanism in the ceramic can be thought of as ballistic phonon propagation through a grain (crystallite), with a probability f_ω that a phonon will pass from one grain to another across an intergranular layer. It is reasonable to think in this case that phonon scattering reflects only the structure and properties of the intergranular layer. If the condition $qR \gg 1$ is also met (where q is the phonon wavenumber), the phonon spectrum of the grain interior is similar to the spectrum of its vibrational excitations, and the grain boundaries can be represented as flat layers of finite thickness d with an acoustic impedance different from that of the grain interior [11].

For $t \gg t_0$ (where t_0 is the time needed for a phonon to cross a grain), the diffusion coefficient in dense ceramics meets the relation $D \propto R^2/t_0$. Given that $t_0 \sim R/(vf_\omega)$, we obtain

$$D \propto Rvf_\omega. \quad (2)$$

It follows from (2) that $D \propto R$ in the proposed model and that f_ω plays a key role in determining spectral characteristics of nonequilibrium phonons, i.e. their $D(T)$. If a phonon wave vector projection is comparable to the inverse intergranular layer thickness, f_ω as a function of grain boundary thickness may exhibit resonance behaviour, i.e. $D(T)$ may both increase and decrease. The problems of evaluating f_ω and determining the acoustic impedance of the intergranular layer were solved by Barabanenkov et al. [11] for a flat boundary of finite thickness.

Figure 2, borrowed from [16], shows the diffusion coefficient D as a function of average grain size for a number of oxide ceramics, including optically transparent ceramics based on cubic oxides, at $T = 3.8$ K and $qR \gg 1$. The solid lines connect data points for ceramics of the same composition. Point A is for an $Y_3Al_5O_{12}$ (YAG) single crystal [6]. The variable parameters were the annealing temperature and time, which determined the average grain size. $D(R)$ shows almost linear behaviour when R is varied by two to three orders of magnitude. This suggests that the properties of intergranular layers may persist in a wide range of process parameters.

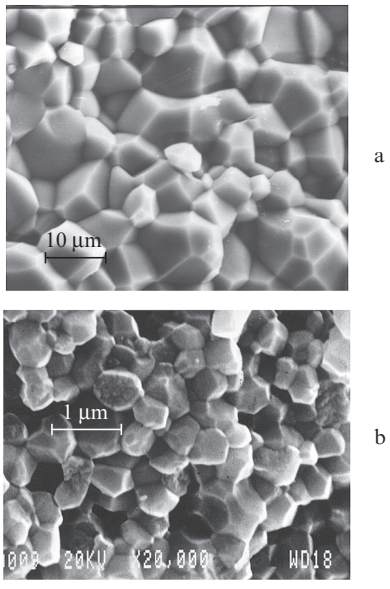

a

b

Figure 1. Fracture surfaces of (a) $Y_3Al_5O_{12}$ (YAG) and (b) $ZrO_2:Y_2O_3$ (YSZ) ceramics.

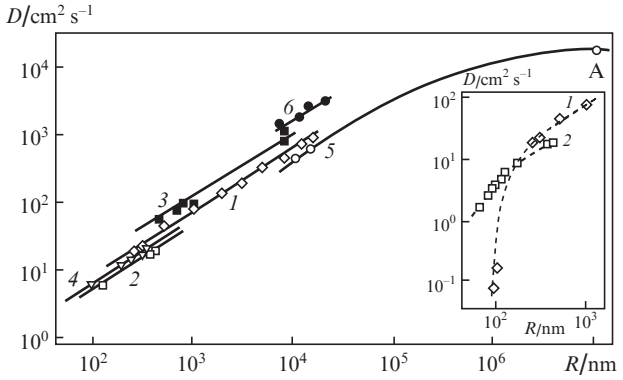

Figure 2. $D(R)$ data at $qR \gg 1$ and $T = 3.8$ K for oxide ceramics based on (*1*) Al_2O_3 [11], (*2*) YSZ [12], (*3*) TiO_2 [13], (*4*) TiO_2 (microwave synthesis) [14], (*5*) YAG and (*6*) Nd:YAG ($C \approx 1\%$ Nd) [15]. Inset: portions of curves (*1*) and (*2*) at $R \sim 100$ nm.

It should be noted that, at liquid-helium temperatures, the transport properties of nonequilibrium phonons in samples with different structures may differ by several orders of magnitude, whereas at room temperature such differences are insignificant. This high sensitivity of the technique is due to the fact that, at low temperatures, inelastic phonon–phonon interactions, which obscure phonon scattering by structural defects, are missing.

3. Analysis of the structure of intergranular layers in oxide ceramics

As an example, Fig. 3 compares estimated acoustic impedances and intergranular layer thicknesses in ceramics based on yttria-stabilised zirconia (YSZ), $ZrO_2:Y_2O_3$, prepared under various conditions at $qR \gg 1$ [12].

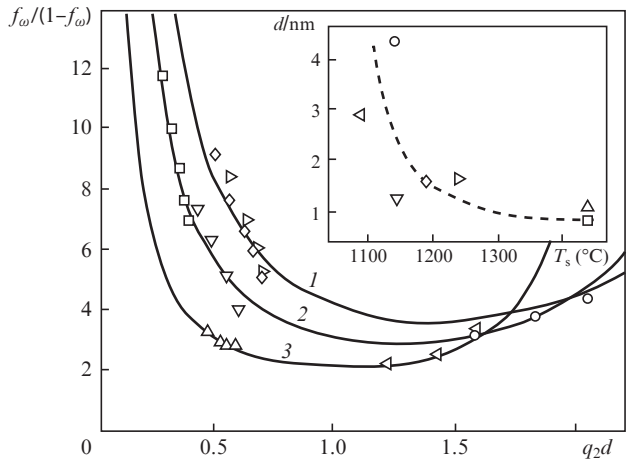

Figure 3. Calculated probability $f_\omega/(1-f_\omega)$ of a phonon flow from one grain to another across a flat grain boundary of thickness d as a function of q_2d at $\rho_2v_2/(\rho_1v_1)$ = (*1*) 0.6, (*2*) 0.7 and (*3*) 0.75. The points represent experimental data. Inset: thickness d as a function of annealing temperature T_s.

The experimental data were analysed using the relation [17]

$$l = l_0 \frac{f_\omega}{1-f_\omega}, \tag{3}$$

where l is the effective phonon mean free path in a layered periodic structure of period R when no scattering occurs in the grain interior. The phonon mean free path in a grain before a scattering event at the grain boundary is $l_0 = 0.6R$ [18].

Figure 3 shows $f_\omega/(1-f_\omega)$ as a function of q_2d (where q_2 is the phonon wavenumber in the intergranular layer) for different ratios of the acoustic impedance of the intergranular layer to that of the grains, $\rho_2v_2(\rho_1v_1)^{-1}$, where ρ_1 and ρ_2 are the densities of the intergranular layer and grains. The curves demonstrate that $f_\omega/(1-f_\omega)$ is a strong function of q_2d, which is the consequence of a resonance mechanism [11] related to the distinction between ρ_2v_2 and ρ_1v_1, as well as to the fact that the inverse intergranular layer thickness, d^{-1}, is comparable to the wave vector projection of the injected phonons. Thus, acting as a resonance structure, the intergranular layer causes the transmission coefficient of a pulse of weakly nonequilibrium phonons to depend on the thermostat temperature. The derivative of this dependence can be both positive and negative.

The $f_\omega/(1-f_\omega)$ versus q_2d calculation results were compared to $l(T)/l_0$ experimental data as follows: For a particular sample at T = 3.8 K, we obtained a section through a set of theoretical curves at the corresponding value of $l(T = 3.8\text{K})/l_0$. The intersection points on the curves corresponding to different $\rho_2v_2/(\rho_1v_1)$ ratios determine a number of q_2d values. Taking $q_2 = 3k_BT/(\hbar v_2)$, we find d. The coordinates of the other points in the temperature dependence of l/l_0 for a given sample correspond to the experimentally determined values of $l(T)/l_0$ and $q_2(T)d$ (for the d value obtained in the preceding step).

The curve that ensures the best fit of the calculation results to the experimental data allows the intergranular layer thickness d and $\rho_2v_2/(\rho_1v_1)$ ratio to be determined. The inset in Fig. 3 shows the temperature dependence of d for the materials under consideration. The intergranular layer thickness evaluated in this way for Y_2O_3: $Nd^{3+}$and Lu_2O_3 ceramics [13, 19] approaches the lattice parameter of the grains. In all cases, we observed general trends when the condition $qR \gg 1$ was met: the phonon diffusion coefficient increased with increasing grain size and decreased with increasing intergranular layer thickness. The assumption that the grain boundary is flat ($qR \gg 1$) implies that the model is only applicable to coarse-grained ceramics. The model is incapable of describing the variation of the phonon diffusion coefficient with grain size, $D(R)$, when R approaches the wavelength of the injected phonons.

To take into account a finite curvature of grain boundaries, Salamatov [20, 21] considered a model in which the properties of an elastic medium of density ρ_0 were described by one elastic modulus, K_0 [scalar model with a dispersion law for phonons of arbitrary polarisation $\omega(q) = v_0q$ ($v_0^2 = K_0/\rho_0$)]. As main scattering centres, he examined spherical shells of outer radius R_g, whose thickness and elastic parameters v_1 and ρ_1 ($K_1 = v_1^2\rho_1$) modelled those of grain boundaries. The material in the shells and beyond modelled ceramic grains. According to our results, resonance scattering by spherical shells at a phonon wavelength $\lambda \approx R_g$ is possible when $K_1/K_0 \ll 1$, and the normalised resonance frequency is

$$x_r = \sqrt{\frac{K_1R_g}{K_0d}} \quad (x = qR_g). \tag{4}$$

Figure 4, borrowed from [22], presents the results of analysis, in the above model, of the frequency dependence of the diffusion coefficient for two model parameters: x_r and c_g (where c_g is the volume fraction of spheres of radius R_g). It is seen that, at low x values, all the curves are indicative of Rayleigh scattering with $D \propto 1/q^4$; at high x values, there is geometric scattering with $D \approx lv_0$ and $l \approx 2R_g/(3c_g)$. Curve (*4*) in Fig. 4 relates to a system containing perfectly hard spheres (well-stabilised boundaries), which do not lead to resonance scattering. In the range $x \sim 1$, changes in the elastic properties of the intergranular layer, which determine x_r, may be accompanied by qualitative changes in the behaviour of the phonon diffusion coefficient, including the formation of a frequency range of low transmission (gap in the phonon spectrum) and a change in the sign of the $\partial D/\partial T$ derivative.

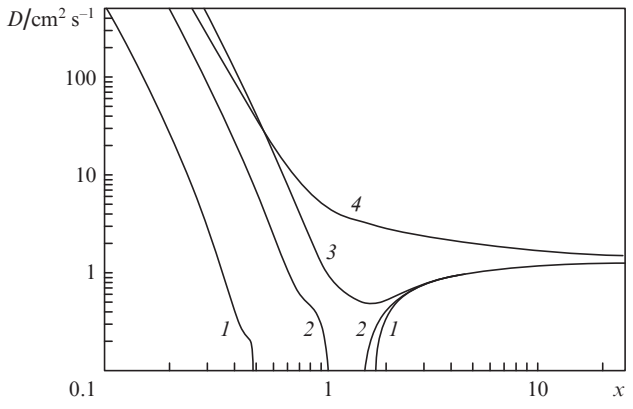

Figure 4. Diffusion coefficient $D(x)$ calculated at $c_g = 0.5$ for resonance frequencies x_r = (*1*) 0.5, (*2*) 1.0 and (*3*) 1.5; (*4*) perfectly hard spheres.

The inset in Fig. 2 presents $D(R)$ data at $T = 3.8$ for two types of ceramics: Al_2O_3 and YSZ. In both cases, $D(R)$ drops sharply at $qR < 20$ ($v = 7.4\times10^5$ cm s^{-1} for Al_2O_3 and $v = 4.33\times10^5$ cm s^{-1} for YSZ), which can be interpreted as evidence for effective scattering of nonequilibrium phonons by ceramic grains at $R \leqslant 100$ nm. The gap in the phonon spectrum at subterahertz frequencies suggests the possibility of $qR \sim 1$, which means that at $q \sim 10^6$ cm^{-1} ($T \approx 3$ K) the grain size should be 20–30 nm.

Single-phase nanostructured ceramics with such a grain size are difficult to prepare. At the same time, one can fabricate composites containing, along with stable grains of a major phase, second-phase nanoinclusions. Such composites, YSZ + 14% Al_2O_3, were prepared by Ivanov et al. [23]. The salient feature of this structure is the presence of a finely dispersed (R = 20–40 nm) metastable phase, corundum. With increasing synthesis temperature T_s, this phase partially converts to a denser phase, α-Al_2O_3 ($\rho_0 = 3.97$ g cm^{-3}), leading to the formation of a countable number of shrinkage nanopores. The presence of even relatively low concentrations of additional nanoscale scattering centres (metastable corundum, shrinkage pores) may lead to significant changes in the phonon spectrum of the material: formation of a gap and shift of its top boundary to higher frequencies (Fig. 5).

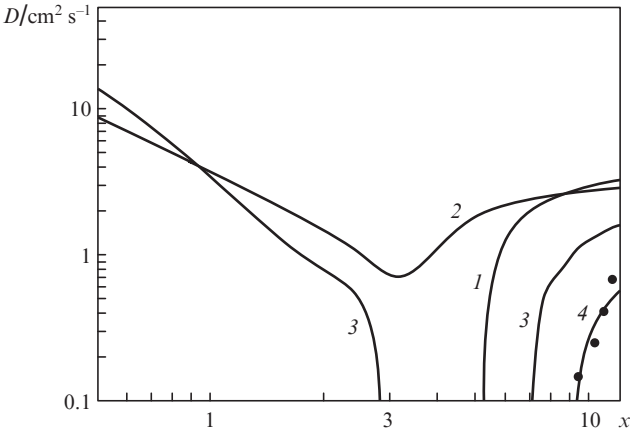

Figure 5. Diffusion coefficient related to (*1*) pores, (*2*) shells of YSZ grains and (*3*) shells of metastable Al_2O_3; (*4*) total diffusion coefficient in the material (experimental data from Ivanov et al. [22]).

The above results reflect the fact that a decrease in grain size, typically caused by a decrease in synthesis temperature and time, leads to an increase in the thickness of the intergranular layer, a decrease in its density and degradation of its elastic properties. As a consequence, the thermophysical properties of the material also degrade. On the other hand, the fabrication of ceramics based on a disordered medium offers the possibility of creating phonon crystals with an effective periodicity parameter determined by the average grain size.

4. Structure of $Y_3Al_5O_{12}$ ceramics

One important achievement in laser physics, solid state physics and optical materials research in the last decade has been the creation of a new class of active functional materials: crystalline laser ceramics based on cubic oxides doped with trivalent lanthanoid ions, Ln^{3+} [24]. According to recent work, lasing characteristics of ceramics depend significantly on the grain size and structure and are influenced by intergranular layers (grain boundaries). In addition, ceramics have been shown to differ little in thermal conductivity from single crystals of the same composition at $T \geqslant 300$ K, whereas their mechanical properties are markedly better than those of single crystals. This refers primarily to the most widely used, YAG-based laser ceramic (see e.g. Ref. [25]).

Even the first experiments concerned with phonon spectroscopy of optically transparent ceramics based on YAG and Nd:YAG [15] showed that the intergranular layer thickness was $d \ll a$, where $a = 1.2002$ Å is the lattice parameter in the grain interior. On the other hand, it was shown that the Nd distribution in some ceramics was nonuniform, because the heavy ions (Nd) were forced out to grain boundaries during synthesis [Fig. 2, curves (*5*, *6*)]. As the synthesis process was improved, the phonon mean free path in YAG ceramics (Konoshima Chemical Co.) approached that in single crystals of Re:YAG solid solutions [26]. As a result, the l/R ratio exceeded 10^2. This is inconsistent with the assumption that the intergranular layer has a finite thickness. The largest phonon mean free path has been achieved in materials prepared by a VSN process ('vacuum sintering and nanocrystalline technology'): precipitation with the use of vacuum sintering at zero external pressure [27]. It seems likely that, in ceramics produced by an optimised process, an 'ideal' grain boundary is a natural crystallographic boundary such as a twin boundary in single crystals.

A comparative analysis of the transport properties and structure of ceramics revealed a number of distinctions, correlated with the grain size. Examination of fracture surfaces by scanning electron and atomic force microscopies showed that samples with a grain size R = 1–2 μm were twinned throughout (Fig. 6a). The twin planes were ~100 nm apart.

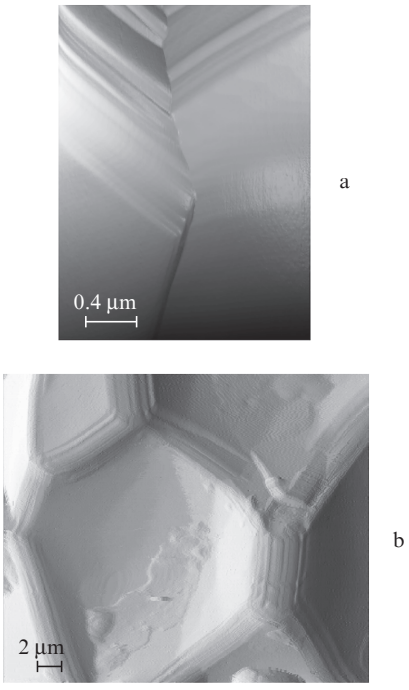

Figure 6. Micrographs of ceramic specimens: (a) intergranular and (b) transgranular fractures.

For $R > 2$ μm, twinning was only observed near grain boundaries or there was no twinning at all (Fig. 6b) [26].

Twinning processes are known to improve structural perfection [28, 29]. A moving twin boundary may effectively eliminate defects in the crystal, making no significant contribution to phonon scattering.

There is some evidence that the defect density and the associated stress in the grain structure increase with grain size. In particular, intergranular fracture prevails at a grain size of 1–2 μm. At a larger grain size ($R \geqslant 10$ μm), transgranular fracture prevails. This is indirect evidence that large grains have lower strength and experience stress. Moreover, the variation of l/R with grain size (Fig. 7) also indicates that the stress increases with R. In the range $R = 1-30$ μm, l/R was found to decrease by two orders of magnitude [26]. For samples with $R = 1-2$ μm and the largest phonon mean free path, prepared through pressureless compaction [27], the trailing edge of the diffusion signal, $S(t)$, asymptotically approached the form $S(t) \propto t^{-1/2}$, characteristic of classic diffusion and a 'planar' phonon source [Fig. 7, inset, curve (*1*)]. Asymptotics of the trailing edge of the signal for $R > 10$ μm showed signal stretching, which might be caused by rereflection from grain boundaries due to extra anisotropy of neighbouring grains [curves (*2*, *3*)]. A theoretical analysis of the diffusive transport of 0.874-THz phonons in dense α-Al_2O_3-based ceramics with zero grain boundary thickness, where scattering was only caused by grain misalignment and elastic anisotropy, was presented by Kaplyanskii et al. [18]. They obtained the following expression for the phonon mean free path:

$$l = l_0 \frac{1}{1 - \langle \cos\alpha \rangle}, \tag{5}$$

where α is the scattering angle of the phonons.

Relation (5) reflects the fact that an increase in the acoustic impedance jump across grain boundaries, due to extra anisotropy in the grain structure, reduces the phonon mean free path and increases phonon reflection, thereby stretching the trailing edge of the signal (Fig. 7). The above results can be interpreted as evidence that, when there is no twinning, the stress in the grain structure increases with grain size, which should degrade the acoustic, thermophysical and optical (depolarisation) properties of the material and is caused by the more severe compaction and synthesis conditions.

The 120° dihedral angles on the fracture surface of a YAG ceramic in Fig. 6b correspond to an ordered grain structure, because cubic structures can form this configuration of crystallographic boundaries only for (111) grain boundaries. Twinning near grain boundaries points to the presence of natural crystallographic boundaries. Another example of an advantageous role of plastic deformation via twinning is the reduction in dislocation density and improvement of the structural perfection of the grains of optically transparent lithium-fluoride-based laser ceramics [7].

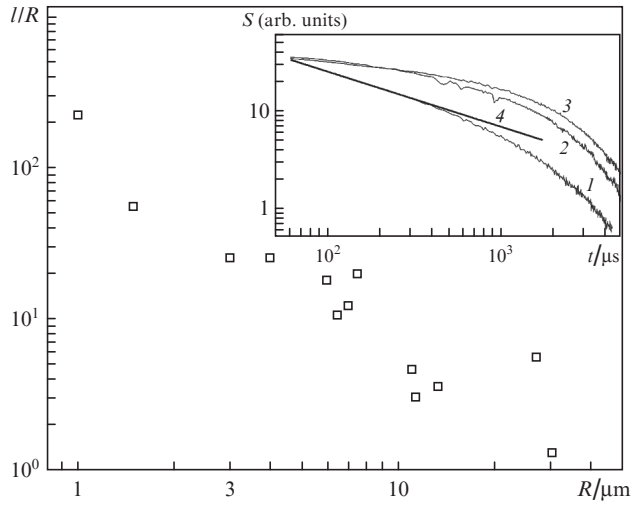

Figure 7. l/R ratio as a function of grain size for YAG ceramics at $T = 3.8$ K. Inset: (*1–3*) asymptotics of the trailing edge of the diffusion signal S measured by the bolometer for Nd:YAG ($C \approx 1\%$ Nd) ceramics; (*4*) $S \propto t^{-1/2}$ asymptote.

5. Conclusions

The study of transport characteristics of nonequilibrium subterahertz phonons in polycrystalline ceramic materials at liquid-helium temperatures is a sensitive method for assessing the degree of stabilisation of grain boundaries in relation to ceramic fabrication conditions.

Plastic deformation via twinning in the structure of grains allows one to improve the thermophysical and optical characteristics of ceramics. The best quality of grain boundaries, stress-free grain structure and, hence, the best acoustic, thermophysical and optical properties of Nd:YAG ceramics can be achieved by precipitation followed by vacuum sintering at zero external pressure, where the main plastic deformation mechanism, responsible for the formation of the grain and grain boundary structure, is twinning and the grain size is within 1–2 μm. The acoustic transmission of ceramics in the terahertz range is comparable to that of single crystals of Re:YAG solid solutions. At liquid-helium temperatures, the ratio of the phonon mean free path to the average grain size, l/R, can reach several hundred, which points to a natural crystallographic character of grain boundaries and indicates that the grain structure is free of stress and defects.

Whether or not the phonon spectrum has a gap, which would degrade the thermophysical characteristics of the ceramic material, is determined to a significant degree by the elastic properties of the intergranular layer. The presence of even relatively low concentrations of second-phase inclusions or pores with a characteristic size less than the grain size shifts the gap to higher frequencies.

Acknowledgements. This work was supported by the Presidium of the Russian Academy of Sciences (Extreme Light Fields and Their Applications Programme) and the Russian Foundation for Basic Research.

References

1. Siegel R.W. *Nanostruct. Mater.*, **4**, 121 (1994).
2. Gusev A.I. *Usp. Fiz. Nauk*, **168**, 55 (1998).
3. Clarke D.R. *J. Am. Ceram. Soc.*, **70** (1), 15 (1987).
4. Ernst P., Kienzle O., Ruhle M. *J. Eur. Ceram. Soc.*, **19** (6-7), 665 (1999).
5. Levinson I.B. *Zh. Eksp. Teor. Fiz.*, **79**, 1394 (1980).
6. Ivanov S.N., Khazanov E.N., Paszkiewicz T., et al. *Z. Phys. B: Condens. Matter*, **99** (4), 535 (1996).
7. Khazanov E.N., Taranov A.V., Gainutdinov R.V., et al. *Zh. Eksp. Teor. Fiz.*, **137** (6), 1126 (2010).

8. Ivanov V.V., Salamatov E.I., Taranov A.V., Khazanov E.N. *Zh. Eksp. Teor. Fiz*., **137** (1), 41 (2010).
9. Von Gutfeld R.J., Nethercot A.H. Jr. *Phys. Rev. Lett.*, **12** (23), 641 (1964).
10. Ivanov S.N., Kosorezov A.G., Taranov A.V., Khazanov E.N. *Zh. Eksp. Teor. Fiz*., **102**, 600 (1992).
11. Barabanenkov Yu.N., Ivanov V.V., Ivanov S.N., et al. *Zh. Eksp. Teor. Fiz*., **119** (3), 546 (2001).
12. Barabanenkov Yu.N., Ivanov V.V., Ivanov S.N., et al. *Zh. Eksp. Teor. Fiz*., **129** (1), 131 (2006).
13. Ivanov V.V., Ivanov S.N., Kaigorodov A.S., Taranov A.V., Khazanov E.N., Khrustov V.R. *Neorg. Mater.*, **43** (12), 1515 (2007).
14. Ivanov V.V., Ivanov S.N., Karban O.V., Taranov A.V., Khazanov E.N., Khrustov V.R. *Neorg. Mater*., **40** (11), 1400 (2004).
15. Barabanenkov Yu.N., Ivanov S.N., Taranov A.V., Khazanov E.N., Yagi H., Yanagitani T., Takaichi K., Lu J., Bisson J.-F., Shirakawa A., Ueda K., Kaminskii A.A. *Pis'ma Zh. Eksp. Teor. Fiz*., **79** (7), 421 (2004).
16. Taranov A.V., Khazanov E.N. *Zh. Eksp. Teor. Fiz.*, **134** (2(8)), 595 (2008).
17. Kagan V.D., Suslov A.V. *Fiz. Tverd. Tela*, **36**, 2672 (1994).
18. Kaplyanskii A.A., Mel'nikov M.B., Feofilov S.P. *Fiz. Tverd. Tela*, **38**, 1434 (1996).
19. Kaminskii A.A., Bagayev S.N., Ueda K., Takaichi K., Shirakawa A., Ivanov S.N., Khazanov E.N., Taranov A.V., Yagi H., Yanagitani T. *Laser Phys. Lett.*, **3** (8), 375 (2006).
20. Salamatov E.I. *Phys. Status Solidi C*, **1** (11), 2971 (2004).
21. Salamatov E.I. *Phys. Status Solidi B*, **244** (6), 1895 (2007).
22. Ivanov V.V., Salamatov E.I., Taranov A.V., Khazanov E.N. *Zh. Eksp. Teor. Fiz*., **133** (2), 339 (2008).
23. Ivanov V.V., Paranin S.N., Khrustov V.R. *Phys. Met. Metallogr.*, **94**, Suppl.1, S98 (2002).
24. Kaminskii A.A., Taranov A.V., Khazanov E.N., Akchurin M.Sh. *Kvantovaya Elektron*., **42** (10), 880 (2012) [*Quantum Electron*., **42** (10), 880 (2012)].
25. Kaminskii A.A., Akchurin M.Sh., Gainutdinov R.V., Takaichi K., Shirakawa A., Yagi H., Yanagitani T., Ueda K. *Kristallografiya*, **50**, 935 (2005).
26. Akchurin M.Sh., Gainutdinov R.V., Kaminskii A.A., Taranov A.V., Khazanov E.N. *Zh. Eksp. Teor. Fiz*., **135** (1), 93 (2009).
27. Yanagitani T., Yagi H., Ichikawa M. Jpn Patent No. 10-101333 (1998); Yanagitani T., Yagi H., Yamasaki Y. Jpn Patent No. 10-101411 (1998).
28. Akchurin M.Sh., Gainutdinov R.V., Kaminskii A.A. *Poverkhnost*, **9**, 78 (2006).
29. Akchurin M.Sh., Galiulin R.V. *Kristallografiya*, **43** (3), 493 (1998).